J Therm Anal Calorim (2010) 99:443–457
DOI 10.1007/s10973-009-0190-5

The influence of mixed anionic composition of Mg–Al hydrotalcites on the thermal decomposition mechanism based on in situ study

Agnieszka Węgrzyn · Alicja Rafalska-Łasocha · Dorota Majda · Roman Dziembaj · Helmut Papp

Received: 24 February 2009 / Accepted: 22 April 2009 / Published online: 19 June 2009

Abstract A series of Mg/Al hydrotalcites with tailored content of carbonate and nitrate anions was prepared using precipitation method. A part of the obtained materials was additionally crystallized in hydrothermal conditions. Different hydrotalcite phases or domains may co-exist within one sample obtained at controlled conditions. Decomposition mechanism studied in situ (DRIFT, XRD) was different for the samples with high concentration of interlayer nitrate anions than for carbonate-containing sample. TG-QMS study of hydrothermally treated samples provided more precise data for quantitative description of decomposition steps of Mg/Al hydrotalcites containing different mixtures of nitrate and carbonate anions.

Keywords Decomposition mechanism · Nitrate-containing hydrotalcite · In situ XRD · In situ DRIFT · TG-QMS

Introduction

Hydrotalcites, or layered double hydroxides, which general formula may be represented as follows: $[M^{II}_{1-x}\,M^{III}_{x}\,(OH)_2]\,A^{n-}_{x/n}\cdot n\,H_2O$, ($M^{II}$, M^{III}—metal cations, A^{n-}—interlayer anion), are versatile inorganic materials studied intensively since they were described and synthesised in the beginning of 20th century [1, 2].

Layered structure, ion exchange properties, high dispersion of elements, flexible chemical composition or so called "memory effect" which is characteristic for hydrotalcite-derived mixed metal oxides, make these materials especially interesting for catalysis, adsorption, pharmacy, medicine and materials engineering [3–5]. Each year new synthetic materials have been described and improved preparation procedures to obtain controlled uniform size or unique shapes of crystallites [6–11].

However, not all questions concerning arrangements of anions within the galleries have been explained. It was observed many times that for nitrate-containing hydrotalcites at high layer charge rearrangement of interlayer anions occurs. Usually this phenomenon had been explained in terms of simple repulsion of anions and its close packing with arrangement perpendicular to brucite-like layers. Only in recent years Xu and Zeng proposed different model [12]. According to their calculations, it is not "tilt-lying" arrangement (nitrates perpendicular to brucite-like layers) but "stick-lying" one (orientation of nitrates is parallel to the layers) that is energetically favoured.

Nevertheless, the described model is not complete because no interlayer water molecules and their interactions with anions were taken into account.

In many applications of hydrotalcite-like materials it is important to understand their decomposition mechanism, in order to prevent excessive sintering or to obtain a metastable active phase. The most common data are available for different carbonate-containing hydrotalcite-like materials, in which thermal stability is a function of metal cations type [13, 14], their atomic ratio [15–17] and, rarely,

A. Węgrzyn (✉) · A. Rafalska-Łasocha · R. Dziembaj
Faculty of Chemistry, Jagiellonian University, Ingardena 3, 30 060 Krakow, Poland
e-mail: wegrzyn@chemia.uj.edu.pl

D. Majda · R. Dziembaj
Regional Laboratory for Physicochemical Analyses and Structural Research, Jagiellonian University, Ingardena 3, 30 060 Krakow, Poland

H. Papp
Institute of Technical Chemistry, University of Leipzig, Linnéstraße 3, 04103 Leipzig, Germany

crystallinity degree [9, 18]. Decomposition process is usually followed by TG analysis in linear thermal programme or differential scanning calorimetry [19], but other techniques such as controlled rate thermal analysis (CRTA) or tapered element oscillating microbalance (TEOM) were also reported [13, 20]. Besides of weight loss and rates of evolved gasses also in situ techniques such as infrared spectroscopy (i.e. DRIFT), XAFS [21] or structural analysis (XRD) may provide valuable data [22–27].

In general, three steps of carbonate-containing hydrotalcites have been described in the literature: dehydration followed by the formation of metastable phase, dehydroxylation of brucite-like layers and decomposition of carbonates resulting in formation of double mixed oxide and/or spinel (after further heating) [21, 28, 29].

Similar steps were observed during thermal evolution of a series of nitrate-containing hydrotalcites [30]. It was also shown that dehydroxylation strongly depends on chemical environment of hydroxyl groups as well as nitrate amount in interlayer spaces.

The aim of our paper is to present differences in thermal behaviour of Mg–Al hydrotalcites containing mixtures of interlayer anions: nitrates and carbonates. We report here description of the structure of tailored mixed nitrate-carbonate containing materials as well as detailed study of their thermal decomposition. Our considerations of decomposition mechanism are supported by the results of in situ measurements (DRIFT, XRD). To the best of our knowledge, no systematic studies were undertaken to understand how carbonate or nitrate impurities may affect thermal behaviour of hydrotalcite-like materials. Moreover, studies on highly crystalline, well defined materials in such research, are sparse.

Experimental

The Mg–Al hydrotalcites containing carbonates, nitrates or a mixture of the anions were prepared using co-precipitation method at constant pH. All chemicals used for the synthesis were of analytical grade (POCh). The solution of $Mg(NO_3)_2 \cdot 6\ H_2O$ (51.2 g, 0.2 mol) and $Al(NO_3)_3 \cdot 9\ H_2O$ (37.5 g, 0.1 mol) in 200 mL of distilled water was added drop-wise to 100 ml of aqueous solution of $NaNO_3$ and/or Na_2CO_3 for nitrate/carbonate-containing hydrotalcites. Low Mg/Al ratio (high layer charge) was chosen due to anions rearrangements in the interlayers of such materials reported before [12]. The amount of carbonates was calculated from the formulae: $[CO_3^{2-}] = 0.05\ [Al^{3+}]$ or $[CO_3^{2-}] = 0.20\ [Al^{3+}]$ for the samples containing a mixture of the anions NO_3^- and CO_3^{2-} compensating the layer charge, or from equation: $[CO_3^{2-}] = 0.75\ [Al^{3+}]$ for the pure carbonate sample. $NaNO_3$ salt was used as a balance instead of chosen amount of sodium carbonate. No sodium carbonate was added in synthesis of nitrate-containing hydrotalcites.

Co-precipitation was carried out at 60 °C under vigorous stirring at pH equal 10.0 ± 0.2. The pH was controlled by simultaneous addition of NaOH (10% aqueous solution) prepared from concentrated (50%) solution directly before synthesis. Obtained suspensions were stirred for 1 h at 60 °C. A part of the obtained suspensions were submitted to hydrothermal treatment at autogenous pressure at 150 °C for 6 days. All the samples were filtered, washed with distilled water and dried at room temperature.

The number in the sample name (i.e. AN54) stands for the percentage of the layer charge compensated by nitrates and letter "A" for hydrothermal treatment.

Chemical bulk analysis was performed using elemental analyser Euro Vector EuroEA 3000 and XRF spectrometer Oxford 2000. Room temperature powder X-ray diffraction patterns of the hydrotalcites were measured by the use of a Philips X'pert PW 3710 diffractometer (CuKα radiation, $\lambda = 1.54184$ Å), while FTIR spectra were recorded with a Bruker IFS 48 spectrometer using the KBr pellet technique. Thermal decomposition was studied in thermobalance Mettler Toledo 851^e connected on-line with a quadruple mass spectrometer ThermoStar Balzers T300. Mass change of the samples (~20 mg) was studied over temperature range 30–1000 °C with heating ratio equal 10 °C min^{-1} in flow of argon (Ar = 80 ml min^{-1}). For the as-prepared and calcined samples TEM pictures were recorded in Philips CM 200 STEM.

High temperature in situ XRD studies were conducted in SEIFERT ID 3000 with XRK Chamber and PSD Detector. XRD patterns were recorded over temperature range from RT to 600 °C in intervals of 25 °C (up to 400 °C) then 100 °C (between 400 and 600 °C). After heating up to desired temperature (heating ratio equal 10 °C min^{-1}) the sample was kept for 30 min at constant temperature.

Diffuse reflectance spectra of thermal decomposition stages were recorded using the infrared spectrometer Vector 22 (Bruker) equipped with Environmental Chamber controlled by a Spectac Eurotherm 2216e controller. Decomposition was conducted in flow of nitrogen (N_2 = 30 ml min^{-1}) in intervals of 25 °C in temperature range 25–400 °C. The spectra were recorded for 3 min at constant temperature and heating rates between measurement points was equal 10 °C min^{-1}. At 400 °C the samples were kept for another 1 h and then last measurement was performed.

On the basis of XRD data, cell parameters a and c were calculated from the formulae given below: $a = 2 \cdot d_{110}$ and $c = (3 \cdot d_{003} + 6 \cdot d_{006})/2$. Additionally, the crystallite size kc and ka were estimated on the basis of the line broadening using Debye-Sherrer equation: $D = kc = ka = 0.89\ \lambda/(\beta \cdot \cos\theta)$.

Results and discussion

Chemical composition

Chemical composition of the series of nitrate/carbonate-containing hydrotalcites determined by XRF and elemental analysis is shown in Table 1. Mg/Al molar ratio in all non-hydrothermally treated samples is close to expected value equal 2. Higher Mg/Al ratios were obtained after hydrothermal treatment. This may result from the fact that the hydrothermal treatment was performed in mother solution characterised by high pH. In such conditions, at high pressure and temperature aluminium cations were susceptible to leaching from the structure. In all the hydrothermally treated samples Mg/Al ratio was equal or higher than 2.30 and maximum value of 2.46 reached for the sample AN54. Because of higher Mg^{2+} content, the calculated layer charge density was lower than expected but still quite high, and the difference between the highest (4.31 e^+ nm^{-2}) and the lowest (3.57 e^+ nm^{-2}) was equal 0.74 e^+ nm^{-2}.

The results of elemental analysis show that obtaining of materials with precisely set NO_3^-/CO_3^{2-} ratio was difficult. High pH of precipitation, different sources of contamination such as NaOH solution prepared without special precautions or prolonged contact with air, may result in incorporation of significant amount of carbonates. It was especially visible in the case of the (A)N21–54 samples. However, as the improvement of the preparation procedure was not our objective, in the mentioned samples the incorporation of nitrates was close to only a half of the expected value. Hydrothermal treatment was also the factor influencing the nitrate/carbonate ratio. In all nitrate-containing samples after treatment, NO_3^- content was higher with respect to un-treated references. Due to incomplete precipitation of all available cations in the course of synthesis at 60 °C, also the number of incorporated anions was different in comparison to the samples submitted to longer crystallization procedure, assuming that carbonates were intercalated in first order.

Water content was changeable, but in general more water molecules were contained in non-hydrothermally treated samples. This might be explained by lower crystallinity of these samples resulting in their higher external surface area. For such solids formation of interparticle cavities filled with water that is difficult to be removed by drying at room temperature may be expected.

RT-XRD

The most representative parts of XRD patterns of the studied samples are shown in Fig. 1. Shift of the positions of the basal reflections to lower angles (9.8–11.6° and 19.8–23.3° 2θ), as a result of the increase of interlayer distance, was correlated with the increasing relative nitrate content. In the case of the samples with medium percentage of NO_3^- (A)N35–54 additional splitting of basal reflection was clearly visible. This indicates coexistence of nitrate-rich and carbonate-rich regions of the structure. Similar effect of the mixed anionic composition was observed also in the case of decavanadate/carbonate hydrotalcite-like materials [31]. The mixture of domains with different basal spacings or co-existing hydrotalcite phases was also the reason of broadening of the reflections. Nevertheless, in each pair of non-treated and hydrothermally treated samples, the latter ones showed more intense patterns. Carbonate-containing hydrotalcites are less soluble than nitrate- or halide-containing materials [32]. This may explain much higher XRD pattern intensity of crystallized AN0 sample than in the other materials.

Anionic composition also influenced the shape of the region containing non-basal reflection (110) of XRD pattern. The increase of nitrate content caused more overlapped (110) and (113) peaks. This feature is often assigned to the lowering of short-range ordering.

Table 1 Chemical composition of Mg–Al hydrotalcites containing different mixtures of nitrates and carbonates

Sample	Formula	Mg/Al molar ratio[a]	Layer charge density/e^+ nm^{-2}	% of layer charge compensated by NO_3^-/%
AN93	$Mg_{0.697}$ $Al_{0.303}$ $(OH)_2$ $(NO_3)_{0.280}$ $(CO_3)_{0.011}$ · 0.520 H_2O	2.30	3.75	93 (100)[b]
N88	$Mg_{0.657}$ $Al_{0.343}$ $(OH)_2$ $(NO_3)_{0.302}$ $(CO_3)_{0.020}$ · 0.889 H_2O	1.92	4.27	88 (100)
AN54	$Mg_{0.711}$ $Al_{0.289}$ $(OH)_2$ $(NO_3)_{0.155}$ $(CO_3)_{0.067}$ · 0.367 H_2O	2.46	3.57	54 (90)
N42	$Mg_{0.683}$ $Al_{0.317}$ $(OH)_2$ $(NO_3)_{0.132}$ $(CO_3)_{0.092}$ · 0.439 H_2O	2.16	3.95	42 (90)
AN35	$Mg_{0.702}$ $Al_{0.298}$ $(OH)_2$ $(NO_3)_{0.104}$ $(CO_3)_{0.097}$ · 0.436 H_2O	2.36	3.68	35 (60)
N21	$Mg_{0.694}$ $Al_{0.306}$ $(OH)_2$ $(NO_3)_{0.066}$ $(CO_3)_{0.120}$ · 0.480 H_2O	2.26	3.81	21 (60)
AN0	$Mg_{0.700}$ $Al_{0.300}$ $(OH)_2$ $(NO_3)_{0.000}$ $(CO_3)_{0.150}$ · 0.471 H_2O	2.33	3.71	0 (0)
N0	$Mg_{0.654}$ $Al_{0.346}$ $(OH)_2$ $(NO_3)_{0.002}$ $(CO_3)_{0.172}$ · 0.645 H_2O	1.89	4.31	0 (0)

[a] Calculated on the basis of XRF analysis

[b] Obtained and (expected) values

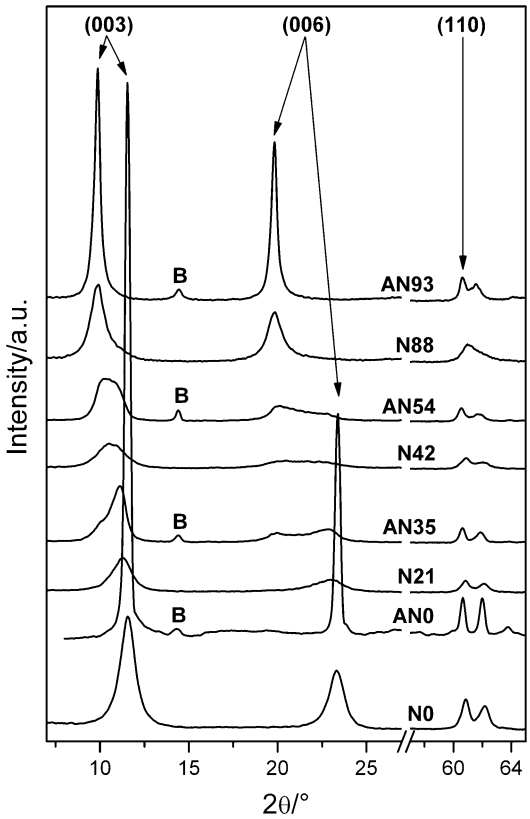

Fig. 1 RT-XRD patterns of Mg–Al hydrotalcites containing different mixtures of nitrates and carbonates; B—boehmite

Another result of prolonged crystallization at elevated temperature and high pressure was formation of impurity phase in the sample series ANx. Two small peaks observed at 2θ equal 14.4° and 28.0° (not shown) indicate the presence of boehmite AlOOH. Nevertheless, the amount of this phase was rather small and should not influence significantly the results obtained in other techniques.

Calculated cell parameters and crystallite sizes are shown in Table 2. The lowest parameter *c* was found for samples (A)N0. The obtained value 22.90–22.93 Å was typical for carbonate-containing samples with high layer charge. Similar value of *c* was obtained for untreated sample N21 (22.84 Å), as one of two extreme values resulting from deconvolution of basal reflections. For the same sample another interlayer distance found was—24.24 Å. Two values of cell parameters *c* were also calculated for AN35, N42 and AN54, the higher one increasing up to 26.61 Å (for AN54). Diversity of cell parameter *c* may result in small asymmetry of basal reflections (but not splitting) as it was observed in the case of the sample N88.

The interlayer distance and *c* of 26.90 Å calculated for AN93 is usually reported for nitrate-containing hydrotalcites with high layer charge and attributed to rearrangement of interlayer anions [12]. Another hypothesis explaining the existence of such high interlayer galleries might be also based on the interactions between anions and brucite-like layers. As it was mentioned above, the number of water molecules changes with the nitrate content. At first it decreases when only small amount of carbonates are replaced by nitrates, then slowly increases with the increase of relative concentration of NO_3^- in interlayers. When only carbonates fill up interlayer galleries there is still space available for water molecules oriented flatly between layers. When a small fraction of carbonates is replaced by nitrates, the anions are more crowded due to lower charge of nitrates. Further replacement of CO_3^{2-} by NO_3^- brings about rearrangement of nitrates. The interlayer distance increases as the less numerous carbonate anions are not able to interact strongly with both adjacent brucite-like layers. A free space available for water molecules appears. The weaker the attractions between anions and brucite-like layers are the more water molecules are intercalated. However it must be stressed, that there are two most common arrangements of anions and in consequence two basal spacings. Described situation does not contradict energetically favoured model of "stick-lying" nitrates reported in literature [12].

Table 2 Cell parameters and crystallite dimensions of Mg–Al hydrotalcites containing different mixtures of nitrates and carbonates

Sample	Parameter *c*/Å	Parameter *a*/Å	Crystallite size[a] (nm)	
			kc XRD	*ka* XRD
AN93	26.90	3.054	42	43
N88	26.89 (24.61)	3.045	17	21
AN54	26.61–23.56	3.059	–	35
N42	26.53–23.28	3.045	–	24
AN35	26.41–23.49	3.055	–	41
N21	24.24–22.84	3.046	–	27
AN0	22.90	3.054	65	56
N0	22.93	3.045	16	31

[a] *kc* crystallite size: *c* axis, and *ka* crystallite size: *a* axis—calculated using Debye-Sherrer's equation

Cell parameter *a* related to intermetallic distances, was much more stable. For all of the non-treated samples it was equal 3.045 or 3.046 Å. For materials after hydrothermal crystallization cell parameter *a* was higher and increased to 3.054–3.059 Å due to leaching of smaller cation (Al^{3+}).

As could be expected the crystallite size *ka*, calculated from broadening of (110) reflections (Table 2.) is higher for carbonate-rich as well as hydrothermally treated materials. On the other hand, *kc* values corresponding to the thickness of the hydrotalcite crystals do not differ considerably. However, in the case of the samples with

inhomogeneous anionic composition it was impossible to calculate the *kc* crystallite sizes on the basis of lines broadening.

RT-FTIR vs. DRIFT

Infrared spectra of the studied Mg/Al hydrotalcites, recorded using two techniques, are shown in Fig. 2. In general the results obtained in transmission and diffuse reflectance modes are similar, but in the latter case the quality of spectra is lower. Higher noise level makes precise analysis difficult especially in the wavenumber range below 600 cm^{-1}. Additionally since the radiation beam in DRIFT mode does not penetrate deep into the sample bed the signal of adsorbed species might interfere with structural components. That is why the range between 1600 and 1200 cm^{-1} consists of broad bands that are difficult for interpretation. The advantage of DRIFT technique is that any special treatment of the samples before measurement (such as preparation of fragile pellets) is required. High temperature experiments are faster and easier than in transmission technique, especially in the case of the samples not transparent enough for IR radiation.

In all recorded spectra it was possible to identify bands assigned to hydroxyl groups, interlayer water molecules and

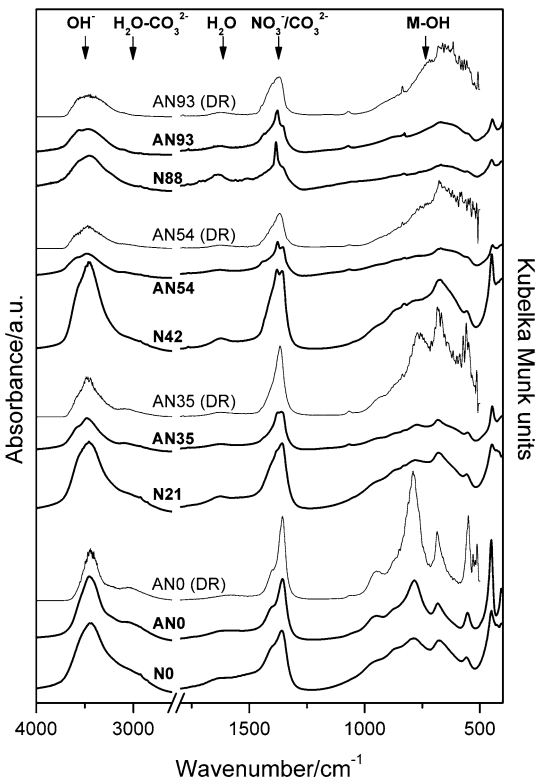

Fig. 2 FTIR vs. DRIFT spectra recorded at room temperature for Mg–Al hydrotalcites containing different mixtures of nitrates and carbonates; DR—diffuse reflectance mode

anions. Stretching vibrations of −OH groups resulted in broad band at around 3500 cm^{-1}. In the spectra of all the samples the main maximum was placed at 3440–3480 cm^{-1}, but additional shoulder was observed at higher wavenumbers. This shoulder is usually assigned as OH groups in Mg_3–OH units while the maximum at 3450 cm^{-1}—as attached to Al^{3+} cations (i.e. Mg_2Al–OH). On the other hand, in our study we observed difference in shoulder position, which is shifted from 3520 cm^{-1} in carbonate-hydrotalcite N0 to 3559, 3563 and 3565 cm^{-1} in the samples with increasing nitrate content N21, N42 and N88. The shift was even higher in the case of hydrothermally treated samples: positions observed for AN35, AN54 and AN93 were 3583, 3590 + 3660 and 3650, respectively. The shape of the whole band changes and its width is the highest for nitrate-rich samples. Clearly, introduction of nitrates results in change of coordination of hydroxyl groups.

Interlayer environment strongly affects also the range in which translation modes of Al–OH and Mg–OH groups are observed, although bands positions change only slightly. Relative intensities of several bands at 950, 870, 780, 670 and 553 cm^{-1} decreased with the increasing nitrate content. On the other hand, two bands at 690 and 620 cm^{-1} became stronger. The shift in position to higher wavenumbers of band the assigned to bending vibrations of interlayer H_2O molecules, from 1620 cm^{-1} observed for N0 to 1635 cm^{-1} for N88 also reflects changing anionic composition and weaker "H_2O–anion" interactions.

As it was reported by Kloprogge et al., no bridging mode is observed between water molecules and nitrates [33]. On the contrary, equivalent band for CO_3–H_2O is present in the spectra of carbonate-rich hydrotalcites, yet its position is shifted from 3030 cm^{-1} for N0 to 3055 and 3068 cm^{-1} for N21 and N42, respectively. Again, the observed relationship is even stronger in the case of hydrothermally treated samples (positions are 3050, 3098, 3109 cm^{-1} for AN0, AN35 and AN54).

Several overlapping bands due to v_3 stretching modes are observed between 1400 and 1350 cm^{-1}. In carbonate-rich hydrotalcites (A)N0–54 their position is 1359–1356 cm^{-1}, while in nitrate-rich samples N88 and AN93 it is shifted to 1356–1355 cm^{-1}. On the other hand, the v_3 modes of NO_3^- appear at 1382 and 1378 cm^{-1} (N21 and AN34) and they are shifted to 1384 cm^{-1} when the highest content of nitrates is reached (N88 and AN93). All described bands are accompanied by shoulders at 1400–1410 cm^{-1} for carbonates and 1420–1435 cm^{-1} for nitrates. Bands positions indicate lowering of the symmetry of carbonates (C_{2v}), while nitrates symmetry is unaltered ($D_{3\ h}$). Complex pattern of broad, overlapping peaks was also recorded in DRIFT mode in the same region. Nonetheless, additional bands confirm the presence of both anions. Stretching mode v_2 of carbonates is observed as band at 870 cm^{-1} and

826–828 cm^{-1} in the case of nitrates. Finally, small sharp peak at 1765 cm^{-1} due to combination of ν_1 and ν_2 modes [34] confirms incorporation of nitrates in samples (A)N21–93. Intensity of the reported band is increasing with increasing concentration of NO_3^-.

TG-DTG-QMS

Total weight loss measured for the series of non-treated hydrotalcites (Nx) increased from 44.7 wt% up to 49.5 wt% with the increasing content of nitrates in the interlayer spaces. It should be easy to understand taking into account their valences. Theoretical weight loss is lower for carbonate- (43.9 wt %) than nitrate-containing sample (50.7 wt %).

The same relationship was observed for the series of hydrothermally treated samples (ANx), although the values were slightly lower and equal 43.6 wt% for AN0 and 47.6 wt% for AN93.

DTG profiles shown in Fig. 3a (solid lines) consist of several broad, overlapping peaks except for the sample N88. Decomposition of the samples N0, N21 and N42 seems to take place in 2 steps below 250 °C and in another two steps between 250 and 600 °C. In the case of nitrate-rich phase (N88) additional distinct decomposition step is observed at around 420 °C. More complex decomposition profiles were observed for hydrothermally treated samples ANx (Fig. 3b). Consecutive decomposition steps are better resolved and narrower.

However, we should rather expect that small particles (low crystalline Nx) would decompose in well resolved stages. Decomposition of bigger crystals would result in overlapping processes, because of diffusion within particles. On the other hand, poorly crystalline materials are not so well defined and high contribution of defects may result in non uniform reaction rate.

Profiles of evolved gasses shown in Fig. 4. follow the same rule. Water molecules are evolved in 4 stages at 146, 236, 312 and 434 °C form carbonate-containing sample AN0. Low temperature transformation is splitted into two maxima at around 100 and 210 °C for the samples AN35 and AN54 and is followed by broader peak consisting of 4 different steps (~300, ~340, ~380 and ~460 °C). On the contrary, in nitrate-rich hydrotalcite AN93 one maximum of low the temperature water loss is clearly separated from other peaks appearing at 345, 381 and 500 °C.

Asymmetric maxima were recorded in case of CO_2 evolution derived form carbonates—one peak with a shoulder for AN0 (447 and 490 °C) and two sharp peaks at around 335 and 380 °C for AN35 and AN54. It is interesting that in the presence of the second anion (NO_3^-) decomposition of carbonates is shifted to lower temperatures—it is almost completed for AN35 and AN54 samples at 430 °C, when only slowly begins in the case of AN0.

Lower temperatures of carbonate decomposition confirm weaker interactions between anions and brucite-like layers. Moreover, according to chemical composition of the hydrotalcites, water molecules evolved below 250 °C

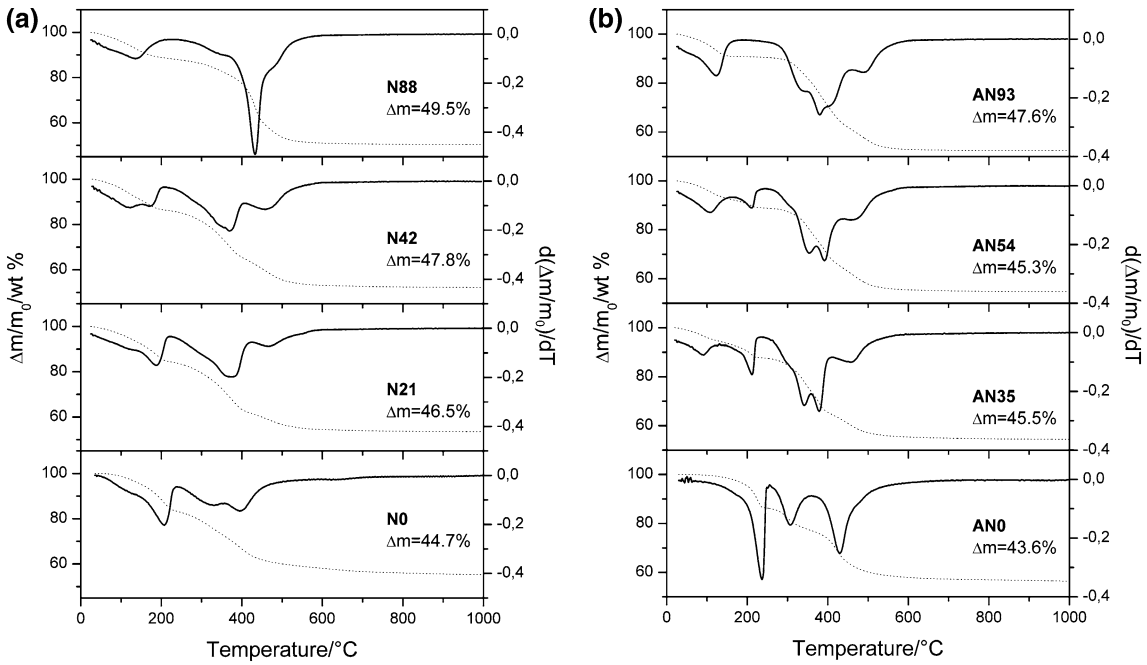

Fig. 3 TG-DTG curves for non-treated (**a**) and hydrothermally treated (**b**) Mg–Al hydrotalcites containing different mixtures of nitrates and carbonates

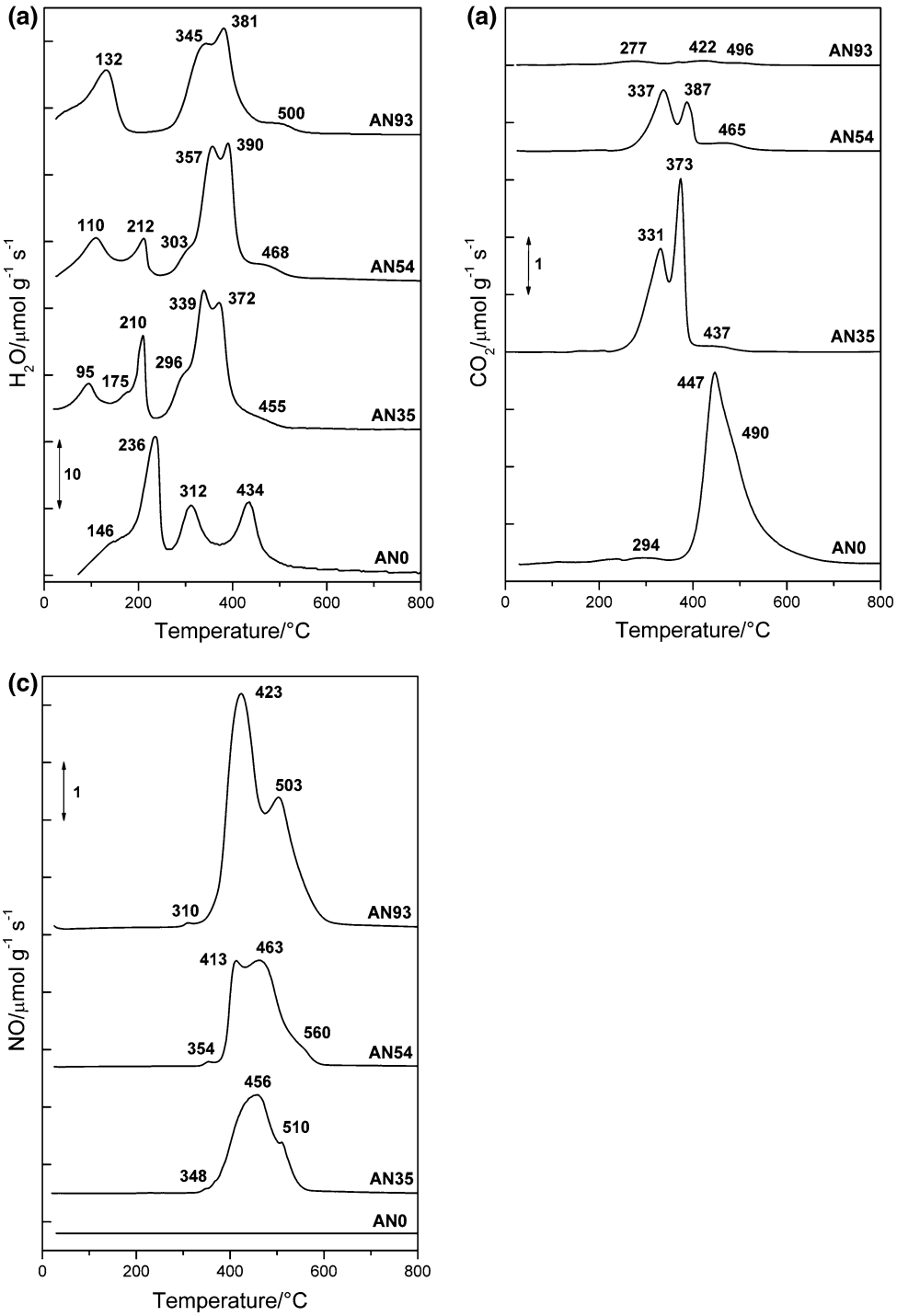

Fig. 4 Evolution of H_2O (**a**), CO_2 (**b**) and NO (**c**) during decomposition of hydrothermally treated Mg–Al hydrotalcites containing different mixtures of nitrates and carbonates

from the sample AN0 come not only from the external surface and the interlayers, but also from partially dehydroxylated brucite-like layers. This process does not result in evolution of carbon dioxide and support hypothesis that before carbonate anions decompose they are grafted in brucite-like layers, what involves partial decomposition of hydroxyl groups. Exact values given in Table 3., show that up to 18% of hydroxyl groups might be decomposed in the course of described process. In temperature range up to 340 °C almost 44% of hydroxyl groups are decomposed while only 5% of carbonates. On the other hand dehydroxylation and decarboxylation occurs simultaneously in other samples.

Anionic composition turned out to be crucial factor of the dehydration process. The more nitrates were incorporated the lower the temperature of dehydration was. 100%

Table 3 Decomposition steps of hydrothermally treated Mg–Al hydrotalcites containing different mixtures of nitrates and carbonates

T[a] (°C)	Amounts of gasses derived from decomposing interlayer water, hydroxyl groups and anions[b]											
	AN0			AN35			AN54			AN93		
	H_2O	CO_2	NO	H_2O	CO_2	NO	H_2O	CO_2	NO	H_2O	CO_2	NO
600–1000		3%	–									
340–600	h: 56%	92%	–	h: 69%	39%	100%	h: 83%	38%	100%	h: 39%	51%	98%
230–340	h: 26%	5%	–	h: 23%	61%		h: 13%	60%		h: 61%	41%	2%
135–230	h: 18%		–	h: 8%			h: 4%	2%			8%	
	w: 100%			w: 36%			w: 22%					
RT-135	[c]		–	w: 64%			w: 78%			w: 100%		

[a] Temperature range includes maximum of the process under discussion

[b] Amounts of decomposed interlayer water (w) or hydroxyl groups (h), carbonates and nitrates are given in percents of total value

[c] Peaks of overlapping two steps

of interlayer water molecules are decomposed below 135 °C in case of nitrate-containing sample AN93, 78 and 64% for AN54 and AN35 respectively. Nitrate decomposition does not start below 300 °C, but when started it takes place in a few abrupt stages between 300 and 500 °C.

According to CO_2 and NO evolution profiles it is possible to distinguish at least 2 different species of carbonate as well as 2 different species of nitrate. In the case of carbonates these species may correspond to flat-lying interlayer anions and grafted molecules. On the contrary, no strong interactions between NO_3^- and brucite-like layers are expected. Probably, some fraction of nitrates may be locked in the structure until decomposition of grafted carbonates is complete and this is the origin of second peak observed at higher temperatures.

Decomposition of NO_3^- results also in simultaneous evolution of O_2, which profiles are not shown because they were exactly the same as those for NO.

In situ HT-XRD

Thermal evolution of the hydrotalcite structure is presented in Fig. 5. Basal reflections of the sample AN0 are sharp and intense below 300 °C, however their splitting is observed at just 200 °C. Two distinct basal distances were calculated, which correspond to flat-lying interlayer carbonates and carbonates grafted to brucite-like layers. Grafting process takes place abruptly without formation of several intermediate phases. At 225 °C only (001) reflections at higher angles remain.

At 300 °C and higher temperatures significant broadening of basal reflections is observed and their consecutive shift to lower 2θ angles. They finally disappear between 400 and 500 °C. Simultaneously non-basal reflections except for (110) are shifted and their intensities decrease up to 300 °C (results not shown). Probably the hydroxide layers still exist at this temperature level despite almost a half of hydroxyl groups are decomposed. All reflections disappear at 400 °C which coincide with CO_2 evolution observed in thermogravimetric analysis. On the contrary to the results reported by Hutson et al. [35], it was impossible to identify $MgCO_3$ phase which was claimed to be one of the intermediates. At 500 °C broad reflections at 43.3 and 62.7° appear, which correspond to MgO phase, in fact solid solution of Al^{3+} cations in MgO matrix.

As it was shown in TG-QMS study, decomposition process of the samples AN35 and AN54 is similar. Strong dehydration at 100 °C results in formation of collapsed structure and XRD pattern consist of sharp intense basal reflections. Nevertheless, upon further heating, when dehydration is complete at around 200 °C, long-range ordering is decreased. Basal reflections become broader and asymmetric, which probably is the result of partial dehydroxylation because of carbonates grafting. At 325 °C, together with the beginning of decarboxylation, (001) reflections are shifted to lower 2θ. Non-basal reflection, except for (110) became weaker at the same temperature range.

Changes of the basal spacing in nitrate-rich sample AN93 are even more complex. As it is shown in Fig. 5d, upon partial dehydration at 100 °C the basal reflections are splitted into several overlapping peaks and shifted to higher 2θ angles. Due to further heating the dehydration process continues and is completed below 200 °C, when narrow sharp symmetric (001) reflections are observed. This might prove that interlayer water molecules play a key role in the formation of expanded basal spacings in nitrate-containing hydrotalcites bearing high layer charge. Some evidence supporting this hypothesis may be driven from calculations of the surface covered by anions in interlayers. NO_3^- and CO_3^{2-} anions geometry is similar and their cross-sections are equal to 0.23 and 0.24 nm^2, respectively [12]. Assuming that each of the layer charges is balanced by

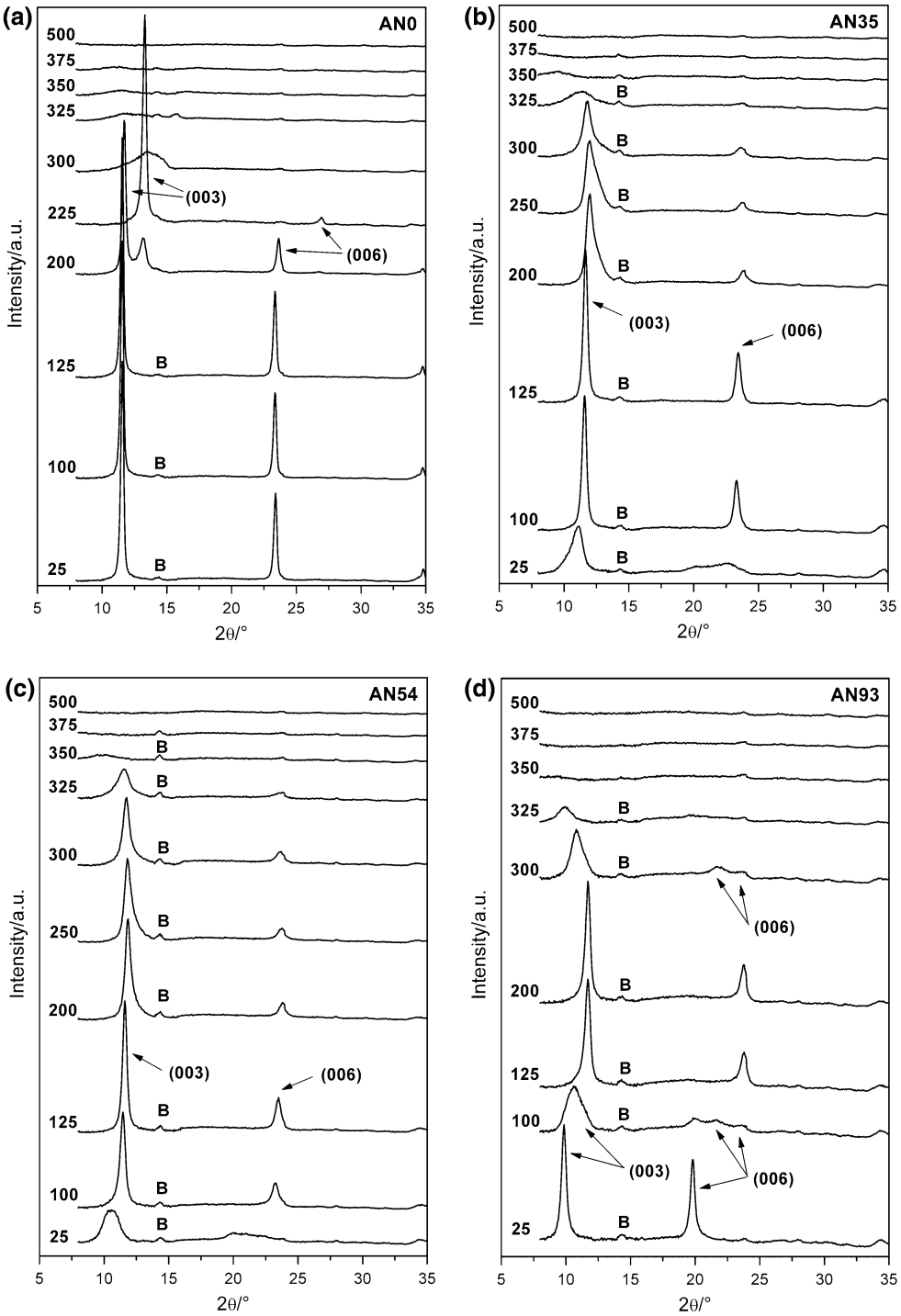

Fig. 5 HT-XRD patterns of hydrothermally treated Mg–Al hydrotalcites containing different mixtures of nitrates and carbonates; evolution of basal reflections for the sample AN0 (**a**), AN35 (**b**), AN54 (**c**) and AN93 (**d**); B—boehmite

equivalent amount of anions (nitrates and/or carbonates) arranged flatly in monolayer, (calculated on the basis of layer charge density per 1 nm^2) the area covered with anions amounts to 0.83, 0.64, 0.59 and 0.45 nm^2 for AN93, AN54, AN35 and AN0, respectively. It means that electrostatic repulsion between anions trapped inside the dehydrated hydrotalcite structure may not be strong enough to change anions arrangement and maintain high basal spacing.

Heating the sample AN93 above 300 °C brings about the increase of basal spacings due to decomposition of the structure components and consecutively weaker attraction between brucite-like layers and anions (results not shown). Intensities of non-basal reflections in the same temperature

range are decreasing. In all nitrate-containing samples formation of MgO phase take place at lower temperature than in carbonate-containing AN0 without formation of amorphous intermediate phase. At 400 °C it is possible to identify peaks at 43.3° and 62.7° 2θ assigned to MgO.

Figure 6 presents evolution of the cell parameter *c* in the series of hydrothermally treated samples. In the case of AN0 *c* is equal to 22.90 Å at room temperature and drops to 19.94 and 19.63 Å at 225 and 300°C, respectively. Assuming layer thickness equal to 4.8 Å, the lowest interlayer distance is 1.7 Å, which is to low to fit carbonate anion in the flat orientation between the layers (2.8 Å). That is why the suggested binding of carbonates to the Mg/Al cations in the layers must occur. Increasing cell parameter *c* at temperatures above 300 °C corresponds to partially decomposed intermediate phase.

In the case of the samples AN35 and AN54 initially several basal reflections corresponding to the range of cell parameters 26.27–23.56 Å and 26.58–23.98 Å, respectively may be found. For both these samples parameter *c* drops in temperature range 100–175 °C to 22.92–22.59 Å for AN35 and 23.08–22.62 Å for AN54. Upon further heating values defining the lowest range of *c* are equal 20.77 Å (AN35) and 21.35 Å (AN54). Finally cell parameter *c* increases up to 27–28 Å. Four different stages of the structure transformation correspond to rearrangement of anions, loss of interlayer water molecules, carbonate grafting and dehydroxylation of brucite-like layers. In the temperature range below 100 °C the structure consists of co-existing hydrotalcite phases or domains, in which low interlayer distances are characteristic for flat-lying carbonates and high values – for nitrates stick- or tilt-lying. Aside these two most common basal spacings several intermediate values are observed. Loss of water molecules between 100 and 200 °C results in formation of an uniform structure with all anions lying flatly in the interlayer galleries. Co-existing

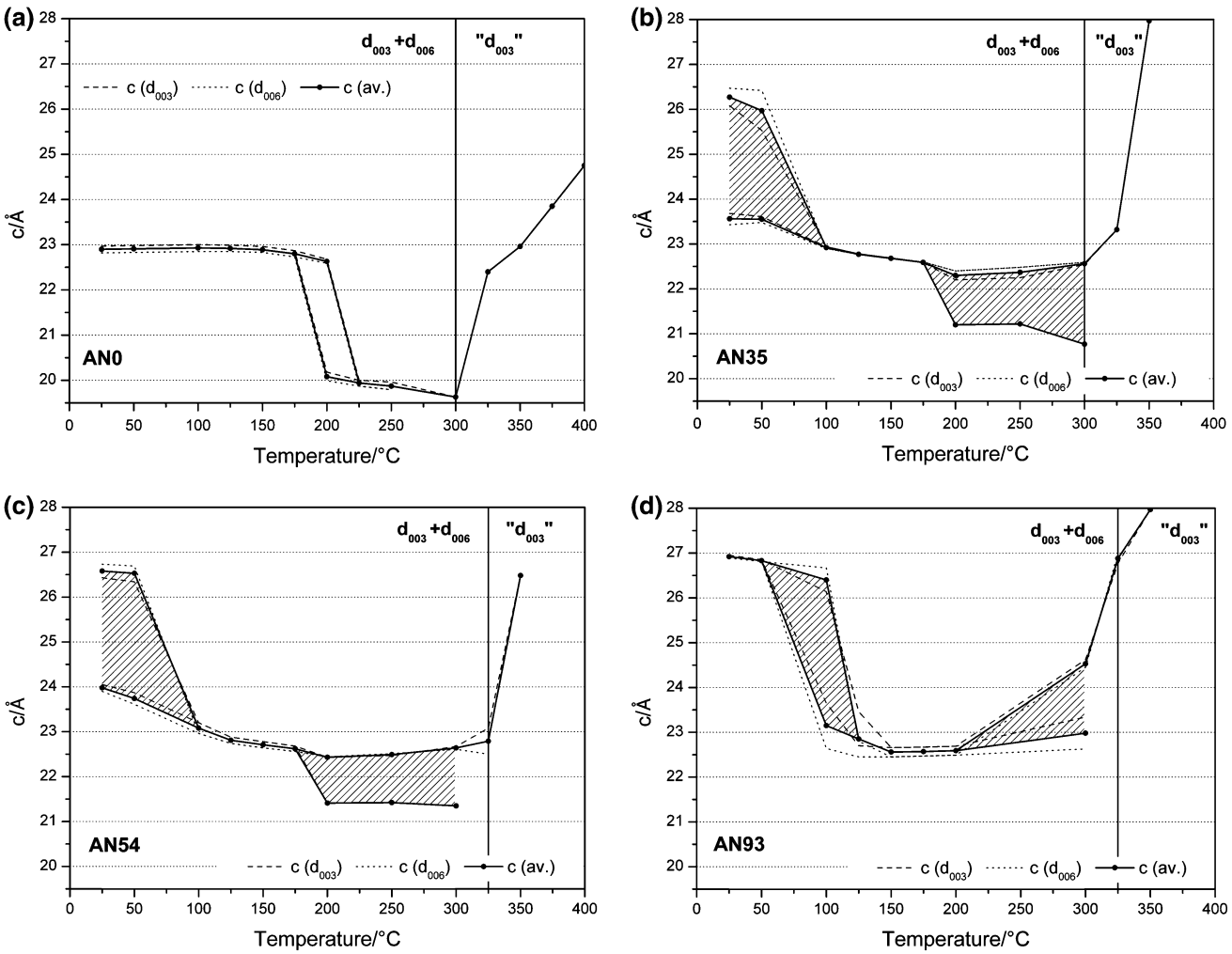

Fig. 6 Evolution of cell parameter *c* for hydrothermally treated Mg–Al hydrotalcites containing different mixtures of nitrates and carbonates: AN0 (**a**), AN35 (**b**), AN54 (**c**), AN93 (**d**)

hydrotalcite phases or domains are observed again between 200 and 300 °C. Low basal spacings correspond to the regions in which carbonates are grafted to brucite-like layers, while high interlayer distances come from flat arrangement of nitrates between partially dehydroxylated layers. Only traces of layered structure remain between 300 and 400 °C.

In nitrate-rich hydrotalcite AN93 decrease of parameter c from 26.92 to 23.15–26.40 Å is observed at 100 °C. Wide range of possible c values confirms the presence of disordered structure with different domains, in which interlayer nitrates have various arrangements between flat-lying and stick-lying depending on the amount of water molecules. Further decrease of the cell parameter c (to 22.56 Å) is observed at 150 °C. This value is close to obtained for carbonate-containing dehydrated hydrotalcite phase in AN0—22.68 Å at 200 °C. Splitting of basal reflections is observed again at 300 °C. Since no significant amount of carbonate is present in the structure, no decrease of cell parameter c occurs. In the studied sample AN93 the range of c varies from 22.98 to 24.53 Å. The increasing value of c between 300 and 400 °C is close to 28 Å. Last two stages correspond to intermediate dehydrated and partially dehydroxylated phases. At the discussed temperature range no significant decomposition of nitrates occurs.

Only small increase of cell parameter a (3.072 Å) was observed up to 300 °C, probably due to thermal expansion of unit cell.

In situ HT-DRIFT

Structural transformations upon heating were studied using DRIFT spectroscopy (Fig. 7). The band of translation vibrations of -OH groups observed for the sample AN0 at 3445 cm^{-1} is shifted to lower wavenumbers at 100 and 255 °C. Additionally new band appeared at 225—250 °C at around 3660–3680 cm^{-1}, while bridging modes H_2O–CO_3^{2-} observed previously at 3045 and 3060 cm^{-1} (25 and 100 °C, respectively) are not present at this temperature range. Splitting of carbonate band at 1344 cm^{-1} into two new bands at 1354 and 1534 cm^{-1} indicates reorganization of the anions and lowering their symmetry [28]. At 400 °C weak band of hydroxyl stretching vibrations is observed at 3588 cm^{-1} and after additional 1 h at elevated temperature—3570 cm^{-1}.

Almost all bands in low range of the spectra of AN0 disappear upon heating: vibration M-OH modes at 948, 790, 550 cm^{-1} and stretching modes of carbonates at 1060, 872, 684 cm^{-1}. Moreover, their position is shifted to lower wavenumbers to 1040, 860, 650 cm^{-1} at 250 °C. The only band that intensity increases is visible at 625 cm^{-1} at 400 °C.

As it was mentioned before, DRIFT mode in comparison to transmission FTIR provides slightly different results. The difference is especially visible between 1800 and 1200 cm^{-1}. The band of bending vibrations of water molecules is shifted or overlapped by peak at 1580 cm^{-1} for the sample AN0. Two bands of v_3 stretching modes of CO_3^{2-} are shifted from 1400 and 1357 cm^{-1} to 1400 and 1344 cm^{-1} at 225 °C. At the same temperature abrupt changes in the spectra occur: broadening of band assigned to translation modes ($\sim$3500 cm^{-1}) and increase of band intensity at 1533 cm^{-1}. These observations agree with total dehydration and partial dehydroxylation (18%) observed in TG-QMS, as well as with the collapse of the structure and the carbonate grafting shown in XRD patterns. Splitted bands 1533–1344 cm^{-1} ($\Delta v_3 = 176$ cm^{-1}) assigned to unidentate carbonate [36] became weaker and are shifted to 1537–1340 cm^{-1} ($\Delta v_3 = 197$ cm^{-1}) at 400 °C and finally 1528–1420 cm^{-1} ($\Delta v_3 = 108$ cm^{-1}) after prolonged heating at the same temperature.

For the sample AN35 the bands below 1200 cm^{-1} assigned to M–OH and carbonate vibrations are not as well resolved as it was observed for AN0. Their positions are shifted from 935, 769, 557 and 1067, 855, 680 cm^{-1} at 25 °C to 940, 755, 560 and 1062, 865, 675 cm^{-1} at 100 °C. Upon further heating the intensity of discussed bands decreases except for one, placed at 875, 868 and 853 cm^{-1} at 250, 300 and 400 °C, respectively.

Decrease of intensity is also observed for the bands assigned to hydroxyl groups vibrations. Moreover, they are shifted from 3470 cm^{-1} (shoulder at 3590 cm^{-1}) to higher wavenumbers up to 3628 cm^{-1} at 400 °C. Bridging H_2O–CO_3^{2-} mode is observed at 3090 and 3100 cm^{-1} at 25 and 100 °C, respectively, then disappears at higher temperatures.

The band assigned to carbonates and/or nitrates stretching vibrations v_3 was found at 1367 cm^{-1} at 25 °C and at lower wavenumbers, 1365 and 1362 cm^{-1}, at 100 and 250 °C, respectively. Between 125 and 300°C new bands of unidentate carbonate stretching modes appear at around 1400–1550 cm^{-1}. One of them, placed at 1426 cm^{-1} at 250 °C is shifted to 1440 cm^{-1} at 300 °C, which is higher position than reported for symmetric stretching mode of unidentate carbonate (1360–1400 cm^{-1}) [36]. Apparently the presence of nitrates changes carbonates symmetry and influences the IR bands positions at lower temperatures. Simultaneously the intensity of the shoulders at 1506 and 1544 cm^{-1} (250 °C), 1550 cm^{-1} (300 °C) increases. These bands are in agreement with values reported for antisymmetric modes. In the same temperature range starts grafting of carbonates and dehydroxylation of brucite-like layers, which results in decrease of basal spacings and evolution of water with distinct maximum at 210 °C.

At 400 °C the bands at 1343–1346 and 1465–1450 cm^{-1} ($\Delta v \cong 120$ cm^{-1}) are assigned to v_3 stretching modes of unidentate nitrate, although their positions are shifted to lower wavenumbers in comparison to the values

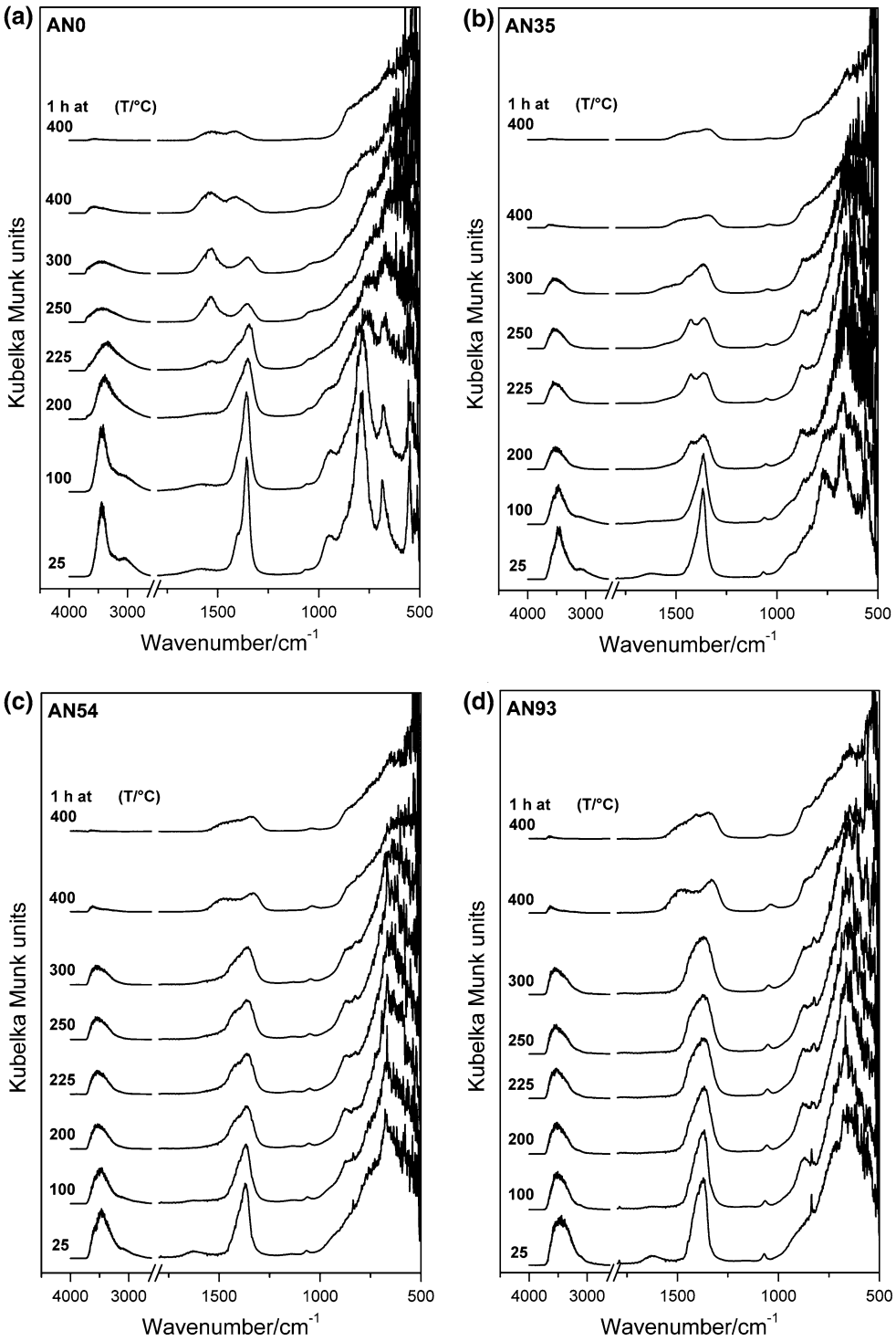

Fig. 7 HT-DRIFT spectra recorded for hydrothermally treated Mg–Al hydrotalcites containing different mixtures of nitrates and carbonates: AN0 (**a**), AN35 (**b**), AN54 (**c**), AN93 (**d**)

reported in literature [37]—1380 and 1490 cm^{-1}. This is with agreement with TG-QMS study, in which it was show that at around 400 °C decomposition of carbonates is almost complete, while evolution of NO only begins.

The increase of nitrates amount in the sample AN54 does not change significantly the spectra character and bands positions between 4000 and 2600 cm^{-1}. Band of hydroxyl stretching vibrations observed at 25 °C at 3466 cm^{-1} with a shoulder at 3580 cm^{-1} is shifted up to 3640 cm^{-1} after 1 h of heating at 400°C. Weak band of bridging H_2O-CO_3^{2-} mode is observed at 3090 and 3105 cm^{-1} at 25 and 100 °C, respectively.

On the other hand, the bands below 1200 cm^{-1} are more overlapped. However, it is possible to find bands assigned

to anions stretching vibrations at 675, 835, 1066 and weak band at 1146 cm^{-1}. Successful intercalation of nitrates is confirmed by the presence of weak sharp band at 1788 cm^{-1}. Upon heating up to 250 °C they are all shifted to lower wavenumbers: 665, 825, 1050, 1130 and 1770 cm^{-1}. Simultaneously, new band appeared at 873 cm^{-1}.

The band described for the sample AN35 and related to unidentate carbonate, is also present in the case of AN54 at temperature range 250–300 °C at around 1420 cm^{-1}, however the intensity is lower. Another band placed at 1565 cm^{-1} appears at higher temperatures (350–400 °C) and should be assigned to unidentate nitrate anions, because only small amount of carbonates remains at discussed temperature range. After additional heating for 1 h at 400 °C the presence of nitrates confirm bands at 1462, 1342 and 1040 cm^{-1}.

Hydroxyl stretching vibrations in the nitrate-containing sample AN93 result in the band that is broader than in the other samples. Moreover in decomposition products spectra it is observed at higher wavenumbers such as 3634 cm^{-1} with a shoulder at 3520 cm^{-1} at 100 °C, 3630 and 3540 cm^{-1} at 250 °C and finally at 3630 cm^{-1} at 400 °C. The shift of the band position to higher wavenumbers in the sample series AN0–AN93 confirms that hydroxyl groups are involved in bond formation with carbonates rather than nitrates. Weak band assigned to bridging H_2O–CO_3^{2-} mode is also shifted to 3100 cm^{-1} at 25 °C and 3120 cm^{-1} at 100 °C.

The bands found at 1070, 836 and 670 cm^{-1} in the spectra recorded at room temperature may be assigned to stretching vibrations of interlayer nitrates. They remain visible up to 400 °C, however shifted slightly to lower wavenumbers: 1038, 810, and 647 cm^{-1}. Strong band appears also at 100 °C at 870 cm^{-1}.

Despite two stages of decomposition process take place between 25 and 200 °C, including 1: partial dehydration resulting in splitting of basal spacings and formation of disordered structure consisting of different hydrotalcite phases or domains, and 2: total dehydration resulting in formation of hydrotalcite containing flat-lying interlayer anions, no evidence of change of nitrates symmetry was found in IR spectra. The band of v_3 stretching modes at 1371 cm^{-1} with a shoulder at around 1400 cm^{-1} remains unchanged up to 200 °C. At 250 °C broadening of the band is observed because of the increasing intensity of the shoulder at 1430 cm^{-1}. Upon further heating two bands are formed at 400°C at 1332 and 1475 cm^{-1}, that are in agreement to reported previously v_3 modes of unidentate nitrate [37]. After additional heating for 1 h at elevated temperature the presence of different nitrate species confirm bands found at 1763, 1482, 1345, 1040, 815 cm^{-1} and new band at 1408 cm^{-1}.

Conclusions

A series of nitrate and/or carbonate containing Mg–Al hydrotalcites was obtained using co-precipitation method (series Nx), additionally followed by hydrothermal treatment (series ANx). Crystallization process affected chemical composition of annealed samples—both parameters, Mg/Al ratio as well as nitrates concentration, increased.

For the two series it was shown that the samples' structure consist of co-existing phases or domains intercalated with carbonate and nitrate anions in different ratio. The presence of nitrates in interlayer spaces brought about rearrangement of the anions and increase of the interlayer spacings depending on nitrates concentration. Moreover, inhomogeneous anionic composition resulted in broadening of basal reflections. Although the crystallite size increased after hydrothermal treatment it was impossible to calculated precise values of crystallite thickness in the case of the samples with mixed interlayer anions.

The presence of both anions was additionally confirmed using infrared spectroscopy.

Thermal analysis showed that decomposition takes place in several steps, that are better resolved in the case of highly crystalline samples. Deconvolution of profiles of evolved gasses (QMS) for the hydrothermally treated samples allowed to calculate precise amounts of water molecules released in the first step of thermal treatment due to dehydration (evolution of interlayer water) and hydroxyl groups that were decomposed due to carbonate grafting. Different chemical environment resulted in two-step decomposition of interlayer carbonates for the samples with a mixed anionic composition.

The results obtained using in situ techniques (XRD and DRIFT) were in agreement with TG/QMS analysis. Complex phase transformation upon heating were described as follows:

- partial dehydration (up to 100°C)—splitting of basal reflections in pure-nitrate sample,
- dehydration (125–200°C)—decrease of basal reflections in nitrate-rich phases, formation of the structure with uniform interlayer distances,
- carbonates grafting followed by partial dehydroxylation (200–300°C)—splitting and decrease of basal reflections in carbonate-containing phases/domains, change of carbonates symmetry,
- carbonates decomposition and further dehydroxylation (300–400°C)—formation of intermediate layered phase, increase of basal reflections,
- nitrates decomposition and formation of MgO phase (400–600 °C), change of nitrates symmetry.

As it was shown, all interlayer molecules such as water, nitrate and carbonate anions, play different role in

formation of the supported hydrotalcite structure. Thermal annealing results in various interactions of these species with brucite-like layers and therefore we may expect different characteristics of decomposition products, i.e. porosity or even distribution of cations. On the basis of the preliminary measurements of N_2 adsorption it was observed that surface area of highly crystalline samples after calcination at 700 °C, was lower than for non-hydrothermally treated counterpart samples. Moreover, there was no simple correlation between anionic composition of the hydrotalcite precursor and surface area of the calcined sample. The lowest value equal 146 $m^2\ g^{-1}$ was obtained for calcined sample AN54 (191 $m^2\ g^{-1}$ for non-hydrothermally treated sample N42), the highest surface area equal 200 $m^2\ g^{-1}$ was measured for AN93 (236 $m^2\ g^{-1}$ for the equivalent non-crystallized sample N88). The detailed discussion of the results of textural properties will be presented in the forthcoming paper.

References

1. Allmann R. The crystal structure of pyroaurite. Acta Cryst. 1968;B24:972–7.
2. Miyata S. US Patent 3 796 792 (1974).
3. Cavani F, Trifiro F, Vaccari A. Hydrotalcite-type anionic clays: preparation, properties and applications. Catal Today. 1991;11: 173–301.
4. Choy JH, Choi SJ, Oh JM, Park T. Clay minerals and layered double hydroxides for novel biological applications. Appl Clay Sci. 2007;36:122–32.
5. Evans DG, Duan X. Preparation of layered double hydroxides and their applications as additives in polymers, as precursors to magnetic materials and in biology and medicine. Chem. Commun. 2006; 485–96.
6. Vial S, Prevot V, Forano C. Novel route for layered double hydroxides preparation by enzymatic decomposition of urea. J Phys Chem Solids. 2006;67:1048–53.
7. Jobbágy M, Regazzoni AE. Delamination and restacking of hybrid layered double hydroxides assessed by in situ XRD. J Coll Interf Sci. 2004;275:345–8.
8. Hu G, O'Hare D. Unique layered double hydroxide morphologies using reverse microemulsion synthesis. J Am Chem Soc. 2005;127: 17808–13.
9. Benito P, Labajos FM, Rocha J, Rives V. Influence of microwave radiation on the textural properties of layered double hydroxides. Microporous Mesoporous Mater. 2006;94:148–58.
10. Benito P, Guinea I, Labajos FM, Rocha J, Rives V. Microwave-hydrothermally aged Zn,Al hydrotalcite-like compounds: influence of the composition and the irradiation conditions. Microporous Mesoporous Mater. 2008;110:292–302.
11. Abelló S, Pérez-Ramírez J. Tuning nanomaterials' characteristics by a miniaturized in-line dispersion-precipitation method: application to hydrotalcite synthesis. Adv Mater. 2006;18:2436–9.
12. Xu ZP, Zeng HC. Abrupt structural transformation in hydrotalcite-like compounds $Mg_{1-x}Al_x(OH)_2(NO_3)_x{\cdot}nH_2O$ as a continuous function of nitrate anions. J Phys Chem B. 2001;105:1743–9.
13. Pérez-Ramírez J, Abelló S. Thermal decomposition of hydrotalcite-like compounds studied by a novel tapered element oscillating microbalance (TEOM). Comparison with TGA and DTA. Thermochim Acta. 2006;444:75–82.
14. Chmielarz L, Kuśtrowski P, Rafalska-Łasocha A, Dziembaj R. Influence of Cu, Co and Ni cations incorporated in brucite-type layers on thermal behaviour of hydrotalcites and reducibility of the derived mixed oxide systems. Thermochim Acta. 2003;395: 225–36.
15. Yun SK, Pinnavaia TJ. Water content and particle texture of synthetic hydrotalcite-like layered double hydroxides. Chem Mater. 1995;7:348–54.
16. Rey F, Fornes V, Rojo JM. Thermal decomposition of hydrotalcites. An infrared and nuclear magnetic resonance spectroscopic study. J Chem Soc Faraday Trans. 1992;88:2233–8.
17. Palmer SJ, Spratt HJ, Frost RL. Thermal decomposition of hydrotalcites with variable cationic ratios. J Therm Anal Calorim. 2009;95:123–9.
18. Hibino T, Yamashita Y, Kosuge K, Tsunashima A. Decarbonation behaviour of Mg-Al-CO_3 hydrotalcite-like compounds during heat treatment. Clays Clay Miner. 1995;43:427–32.
19. Frost RL, Martens W, Ding Z, Kloprogge JT. DSC and high-resolution TG of synthesized hydrotalcites of Mg and Zn. J Therm Anal Calorim. 2003;71:429–38.
20. Vagvölgyi V, Palmer SJ, Kristof J, Frost RL, Horvath E. Mechanism for hydrotalcite decomposition: a controlled rate thermal analysis study. J Coll Interf Sci. 2008;318:302–8.
21. van Bokhoven JA, Roelofs JCAA, de Jong KP, Koningsberger DC. Unique structural properties of the Mg-Al hydrotalcite solid base catalyst: an in situ study using Mg and Al K-edge XAFS during calcination and rehydration. Chem Eur J. 2001;7:1258–65.
22. Kanezaki E. Thermal behavior of the hydrotalcite-like layered structure of Mg and Al-layered double hydroxides with interlayer carbonate by means of in situ powder HTXRD and DTA/TG. Solid State Ionics. 1998;106:279–84.
23. Kanezaki E. Direct observation of a metastable solid phase of Mg/Al/CO_3-layered double hydroxide by means of high temperature in situ powder XRD and DTA/TG. Inorg Chem. 1998;37:2588–90.
24. Millange F, Walton RI, O'Hare D. Time-resolved in situ X-ray diffraction study of the liquid-phase reconstructitm of Mg-Al-carboaate hydrotalcite-like compounds. J Mater Chem. 2000;10: 1713–20.
25. Yang W, Kim Y, Liu PKT, Sahimi M, Tsotsis TT. A study by in situ techniques of the thermal evolution of the structure of a Mg-Al-CO_3 layered double hydroxide. Chem Eng Sci. 2002;57: 2945–53.
26. Kim Y, Yang W, Liu PKT, Sahimi M, Tsotsis TT. Thermal evolution of the structure of a Mg-Al-CO_3 layered double hydroxide: sorption reversibility aspects. Ind Eng Chem Res. 2004;43:4559–70.
27. Pérez-Ramírez J, Abelló S, van der Pers NM. Memory effect of activated Mg-Al hydrotalcite: in situ XRD studies during decomposition and gas-phase reconstruction. Chem Eur J. 2007;13: 870–8.
28. Pérez-Ramírez J, Mul G, Kapteijn F, Moulijn JA. In situ investigation of the thermal decomposition of Co-Al hydrotalcite in different atmospheres. J Mater Chem. 2001;11:821–30.
29. Abelló S, Medina F, Tichit D, Pérez-Ramírez J, Groen JC, Sueiras JE, et al. Aldol condensations over reconstructed Mg-Al hydrotalcites: structure-activity relationships related to the rehydration method. Chem Eur J. 2005;11:728–39.
30. Xu ZP, Zeng HC. Decomposition pathways of hydrotalcite-like compounds $Mg_{1-x}Al_x(OH)_2(NO_3)x{\cdot}nH_2O$ as a continuous function of nitrate anions. Chem Mater. 2001;13:4564–72.
31. Węgrzyn A, Rafalska-Łasocha A, Dudek B, Dziembaj R. Nanostructured V-containing hydrotalcite-like materials obtained by non-stoichiometric anion exchange as precursors of catalysts for

oxidative dehydrogenation of n-butane. Catal Today. 2006;116: 74–81.
32. Allada RK, Pless JD, Nenoff TM, Navrotsky A. Thermochemistry of hydrotalcite-like phases intercalated with CO_3^{2-}, NO_3^-, Cl^-, I^-, and ReO_4^-. Chem Mater. 2005;17:2455–9.
33. Kloprogge JT, Wharton D, Hickey L, Frost RL. Infrared and Raman study of interlayer anions CO_3^{2-}, NO_3^-, SO_4^{2-} and ClO_4^- in Mg/Al-hydrotalcite. Am Mineral. 2002;87:623–9.
34. Kloprogge JT, Ruan H, Frost RL. Near-infrared spectroscopic study of basic aluminum sulfate and nitrate. J Mater Sci. 2001; 36:603–7.
35. Hutson ND, Speakman SA, Payzant EA. Structural effects on the high temperature adsorption of CO_2 on a synthetic hydrotalcite. Chem Mater. 2006;16:4135–43.
36. Di Cosimo JI, Diez VK, Xu M, Iglesia E, Apesteguia CR. Structure and surface and catalytic properties of Mg-Al basic oxides. J Catal. 1998;178:499–510.
37. Miyata S. The syntheses of hydrotalcite-like compounds and their structures and physicochemical properties I: the systems Mg^{2+}-Al^{3+}-NO_3^-, Mg^{2+}-Al^{3+}-Cl^-, Mg^{2+}-Al^{3+}-ClO_4^-, Ni^{2+}-Al^{3+}-Cl^- and Zn^{2+}-Al^{3+}-Cl^-. Clays Clay Miner. 1975;23:369–75.